

Semantic 3D Grid Maps for Autonomous Driving

Ajinkya Khoche^{1 2}, Maciej K Wozniak¹, Daniel Duberg¹ and Patric Jensfelt¹

Abstract—Maps play a key role in rapidly developing area of autonomous driving. We survey the literature for different map representations and find that while the world is three-dimensional, it is common to rely on 2D map representations in order to meet real-time constraints. We believe that high levels of situation awareness require a 3D representation as well as the inclusion of semantic information. We demonstrate that our recently presented hierarchical 3D grid mapping framework UFOMap meets the real-time constraints. Furthermore, we show how it can be used to efficiently support more complex functions such as calculating the occluded parts of space and accumulating the output from a semantic segmentation network.

I. INTRODUCTION

Mapping is essential for autonomous driving. A map of the environment can be used to establish situational awareness, localize the autonomous vehicle (AV), plan safe trajectories taking into account the geometry of the road, traffic rules, and the position of surrounding objects [1], [2]. Endowing the map with semantic information can further enhance understanding of the surrounding environment [3]. If the map is to contribute to the tasks above, the system has to have the ability to analyze the map in *real-time*. This is not trivial to achieve. All data structures and operations to store and access the map must be lightweight and computationally efficient. Several modern AV systems have *pre-built* maps on-board, referred to as HD (high definition) Maps. These maps simplify real-time calculations by providing useful priors [4]. However, building and maintaining these maps so that they are up-to-date is expensive and requires complex algorithms and large computational resources [5].

Regarding the map format, most mapping frameworks store information in 2D grids or in vectorized form. This usually entails rejecting or simplifying some information, e.g., casting 3D readings into 2D. This also means that some information needed to analyze the long-term complex interactions between dynamic agents is discarded from the map, and has to be handled through dedicated object detection and tracking pipelines. These often work in isolation from the mapping process, acting only on the last few sensor frames.

Although 3D semantic mapping algorithms that satisfy real-time constraints are widely used *indoors*, the large scale and complexity of the *outdoor* environment still poses a



Fig. 1: UFOMap with 10 cm voxel size processing 10 hz data from sequence 00 of SemanticKITII [6] dataset in less than 40 ms per sensor frame (single threaded). Top: Full view of the produced map. Bottom: Zoomed in on part of the map.

major challenge. In this paper, we demonstrate that high-resolution dense semantic mapping for AVs is *possible* in real time, using the recently proposed UFOMap [7]. We also believe that a 3D grid may act naturally as an upstream representation from which task-specific representations can be derived. Furthermore, we show an additional benefit that this representation can provide, by acting as a medium for information fusion.

In this paper, we make the following contributions:

- 1) We survey the literature for map representations in autonomous driving.
- 2) We demonstrate that, recent advances in grid mapping allow for dense, high-resolution, real-time 3D mapping in autonomous driving.
- 3) We demonstrate how the semantic information can be used to, on-the-fly, manipulate the map information. This would allow support for downstream tasks with different requirements from a common representation.
- 4) We demonstrate how the map provides the means for sensor / information fusion, exemplified by evaluation on LiDAR based semantic segmentation.

¹KTH Royal Institute of Technology, Stockholm 10044, Sweden. {khoche, maciejw, dduberg, patric}@kth.se

²The author is employed at Scania CV AB, 151 87 Södertälje, Sweden. ajinkya.khoche@scania.com

This work was supported by PROSENSE (2020-02963) funded by VINNOVA, and by the Wallenberg AI, Autonomous Systems and Software Program (WASP) funded by the Knut and Alice Wallenberg Foundation



Fig. 2: Zoomed in on parts of the map shown in Figure 1, demonstrating dense, high-resolution 3D mapping.

II. MAP REPRESENTATIONS

In this section, we provide a brief overview of different types of map representations and the information stored in them. Figure 3 presents a non-exhaustive listing of representations. Depending on the view one takes, one can arrive at slightly different partitioning, and some methods fall in-between groups.

Two key requirements for subsystems used in an autonomous driving setting are computational efficiency and robustness. Autonomy requires that frames can be processed at a speed that matches the rate at which sensors generate data (i.e., between 10 and 40 FPS [8]). Processed here means going from the sensor reading, the analysis of it, deciding which action to take next, and sending the correct signal to, e.g., a throttle or steering unit.

A. HD maps

The requirement for robustness in the mapping process has led to some map information being generated offline and acting as priors during a mission. *HD Maps* are used to model, for example, the geometry and topology of the road (connectivity between the road segments). This includes lane boundaries, center lines, successor-predecessor relationships, speed limits, or directions [9].

Most of the early work relied on manual annotation [10] and only recently this process was automatized [11]. OpenDRIVE, one of the first formats proposed to systematize road description for driving simulators, used *clothoids* to model road segments [12]. However, representing connectivity in this way proved to be cumbersome. Bender *et al.* [10] represented the bounds of the left and right lane using polylines, which also allowed them to implicitly represent connectivity. Their format, called *Lanelets*, allowed encoding driving rules (called regulatory elements) in complex scenarios like intersections and merging. Lanelets were further extended to include physical objects (e.g., road markings, crash barriers) and areas with restricted movement (e.g., parking, sidewalks or buildings) [13]. Lanelet and its extension are lightweight and have been widely adopted for a variety of tasks, such as reachability analysis [14], scenario generation [15] and benchmarks for motion planning [16] or interaction [17].

B. Feature maps

Feature maps store a sparse description of the environment in a form of features extracted from sensor data and their location in space. The extracted features depend on the sensors and the application targeted. Traditionally, image-based features such as edges and corners have been widely explored. The features are often accompanied with a descriptor that simplifies matching. Recently, *Deep Neural Networks* (DNN) are used to extract and learn feature representations [18], [19]. Such approaches can be used for robust re-localization under different lighting or weather conditions [20]. Feature maps support localization related tasks well, but are ill-suited for most other tasks as they provide a sparse representation of objects/obstacles and do not represent free space at all.

C. Dense point clouds

Dense point cloud maps can be obtained by aligning LiDAR point clouds and the corresponding poses. Many

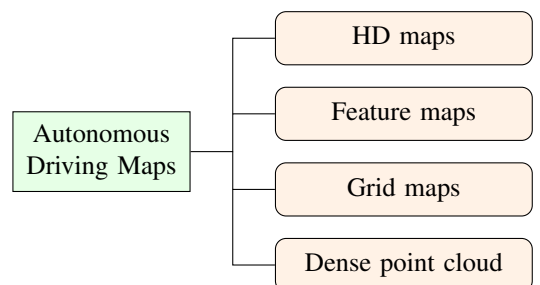


Fig. 3: A non-exhaustive overview of different map representations used in autonomous driving. HD maps are used to store map prior information, such as the location of lanes and drivable areas. Feature maps are commonly used for localization purposes and contain pose-descriptor pairs for landmarks. Grid maps discretize the world and are typically built online from sensor data and used as input for planning. In autonomous driving 2D grids are common, but 3D versions are rare because of the computational cost. Using the point clouds produced by, e.g., a LiDAR as the map representation is also common.

approaches have been developed within the area of LiDAR odometry and mapping [21]. Zhang *et al.* achieve real-time LiDAR odometry and mapping by alternating between a fast scan-to-scan and a slower scan-to-map matching process [22]. Recent work has been aimed at improving the robustness of this solution by adding visual odometry as a prior [23], or matching efficiency by projecting 3D points to range images or bird's eye view [24]. Others choose *surfel-based map* representation due to the ease of rendering [25]. However, a major drawback of using dense point cloud representation is the lack of scalability, owing to high memory consumption, often preventing researchers to use it in applications for autonomous driving.

D. Grid maps

Grid maps were proposed by Moravec and Elfes [26] and have been refined over the years. The basic idea is to discretize space into 2D or 3D grid cells. In autonomous driving applications, it is common to choose a 2D representation as it is less computationally expensive and easier to implement and maintain [27]. 2D occupancy grids are widely used to model free/occupied space used by a planning algorithm to compute a safe trajectory.

A middle ground is a 2.5D representation. An example is the elevation map, modeling the ground height. In [28], each cell of the 2D grid stores a Gaussian mixture model capturing the distribution of data along height at the corresponding position. Another way to represent that are *sticks* presented in [29]. Here voxels with the same feature value are merged along the height direction. It is thus essentially a 2D grid with “sticks” representing the data. *Stixels* [30] similarly are superpixels, defined by clustering points with the same semantic class label in the columns of an image. They proved to be useful and efficient in both static and dynamic environment settings [31].

One relatively common map format under the umbrella of HD maps are rasterized maps, which are essentially *2D grids*. The *NuScenes* dataset [32] encodes drivable areas and sidewalks at a resolution of 10 px/m. *Argoverse* [33] provides masks for drivable areas and ground height, both at one meter resolution. Using the ground height map, false object detection from LiDAR data can be significantly reduced.

When extending grids to 3D, the cells are referred to as voxels. Typically, fixed sized voxels are allocated dynamically and organised using the voxel hashing algorithm. Voxblox [34] is an example of this, storing the truncated signed distance function (TSDF) for each voxel. However, Voxblox struggles when the environment size increases. An efficient way to represent 3D information is using an *octree*. An octree recursively partitions the space till a smallest resolution (chosen as a design parameter) is reached. The inherently hierarchical structure enables performing efficient searches at different resolutions. By prioritizing memory allocation for space with more information, it also provides an efficient way to grow the map. OctoMap [35] is a widely used 3D mapping framework based on octrees, with applications

to planning, exploration and localization tasks. On the other hand, OctoMap is still relatively slow when it comes to updating and accessing the information. UFOMap [7], also based on octrees, overcomes these shortcomings in OctoMap while also adding new features, as seen in Section V.

III. ADDITIONAL MAP USE CASES

As seen in previous section, maps are most often aimed at localization, path planning, and decision making. This section lists some other use cases for maps.

A. Semantic Mapping

In computer vision, semantics is the ability to classify background and foreground [36]. Semantic segmentation methods using DNN acting on camera and LiDAR data can be used to directly annotate dense maps, feature maps, and grid maps [37]. This allows using the same output for multiple tasks, for example, drivable area detection or road landmark detection [11]. Recently, researchers have also achieved promising results in instance-level tracking [38].

However, neural networks are only trained on a fixed number of classes predetermined by the authors of the dataset, which can create the following problems. For instance, a certain group might be interested in segmenting different types of vehicle (e.g., car, truck, ambulance, bus, police), while another group might be satisfied with grouping all the vehicles under one label. One could think of a map as a way to maintain such different views of semantics.

B. Information Fusion

An AV usually fuses information from multiple sensors to achieve robustness. In general, there are two types of fusion processes: late fusion and early fusion. In late fusion, the information is first processed at the sensor level and then fused. On the other hand, for early fusion, the sensor data is first fused together and then processed.

Sensor fusion can also occur over time by combining the readings acquired at different times and positions. Consider again the example of using DNN to estimate semantic segmentation. Researchers often limit themselves to using single images or LiDAR scans as input. Observing that there is a sufficient overlap between measurements, it should be reasonable to expect that fusing successive estimates of the neural network, as the vehicle moves forward, should improve overall semantic segmentation. Although researchers have investigated this idea, they often limit applications to indoor environments [39]–[41] or 2D representations of outdoor environments [11], [42], [43].

Given that the world is 3D, projecting things down to 2D causes information loss and creates a simplified map that makes it difficult, for example, to track temporally occluded objects or estimate the 3D pose of moving objects [44]–[46]. We argue that a 3D grid is ideal for information fusion. Furthermore, a 3D model of the world would provide a better model for occlusions and also allow, for instance a better understanding of pedestrians' behavior [47] or off-road terrain [48], [49].

IV. LIMITATION OF CURRENT METHODS

The map representations described in Section II may be robust or computationally efficient but are designed around specific applications, making it hard to use them for any other task. To enable advanced vehicle autonomy, we believe that map representations should satisfy two more requirements: *flexibility* and *ease of use*.

Maps cater to a variety of downstream tasks, the nature and structure of which can change over time. Flexibility refers to the ability of the mapping framework to adapt to these changes. Failure to do so limits their usability, or worse, risks future development being constrained by the mapping framework design. In order to be easy to use, the mapping framework should enable fast access to information of interest. It should also provide users an intuitive way to query for said information. To our knowledge, none of the existing mapping frameworks for autonomous driving fulfill these requirements, while also being dense, 3D, and satisfying real-time constraints. In the experiments, we show that UFOMap [7] can fulfill these requirements.

V. UFOMAP MAPPING FRAMEWORK

In this work, we build on the UFOMap 3D grid mapping framework¹. In the following, we provide a brief overview for convenience. UFOMap uses the octree data structure. The voxel at the highest resolution is called the *leaf node*, and is used to store occupancy. The sensor data is integrated into the map using ray-tracing, i.e. a ray is projected from the sensor origin and the probability of occupancy at leaf node corresponding to the measured point is updated, while the other leaf nodes along the ray are marked as free. This update function can be user-defined. By default, the fusion scheme mentioned in [35] is used:

$$L(n|z_{1:t}) = L(n|z_{1:t-1}) + L(n|z_t) \quad (1)$$

where

$$L(n|z_t) = \log \left[\frac{P(n|z_t)}{1 - P(n|z_t)} \right] \quad (2)$$

here $P(n|z_t)$ is the occupancy probability for leaf node n given measurement z_t , derived from the beam-based inverse sensor model, and $L(n|z_t)$ is its log-odds value. UFOMap derives its name from the ability to explicitly represent the unknown space, alongside free and occupied space. This is achieved by placing two thresholds on the occupancy probability. Implementing fast integrators and incorporating thread safety allows UFOMap to insert or delete information many folds faster than OctoMap [7].

In addition to occupancy, UFOMap has the ability to store color, semantics, and the timestep information for each voxel. The timestep at every leaf node indicates how recently a given voxel was updated, as shown in Figure 4. The semantics is stored as a dynamically allocated array of label-value pairs. This allows UFOMap to store multiple semantic labels per voxel, as well as gives the user the flexibility to

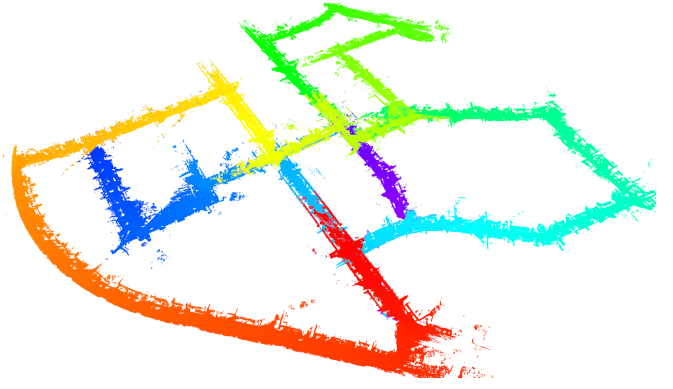


Fig. 4: Same as Figure 1, but showing the time step stored in the voxels. Blue to red color imply older to newer time steps.

expand the list of possible semantics. The label corresponds to the semantics, and the value is an arbitrary quantity attached to a label. In this work, the value represents the number of times a label has been observed. To integrate semantic information, Equation 1 is applied to the top-1 label, $l_{\text{top-1}}$, of each point in a measurement, which means that the value of the label $l_{\text{top-1}}$ in the voxel increases while the values of the other labels remain unchanged.

UFOMap can efficiently query for information based on both the spatial location and the content itself. For example, one could look for all “cars” or “pedestrians” within a 100 m radius of the ego vehicle. These queries can also be made at multiple resolutions. For this, information is propagated so that coarser voxels can summarize information in their children. This propagation function can also be user defined.

VI. EXPERIMENTAL SETUP

In this section, we present experiments to demonstrate dense semantic 3D mapping in real time. We address the limitations described in Section IV and show some examples on SemanticKITTI dataset [6]. LiDAR point clouds, where each point is enriched with color and top-1 semantic label, are fed to UFOMap at 10 hz using ROS [50]. When a new sensor measurement arrives, the probability of occupancy as well as semantics for a leaf node is updated according to Equation 1. Figure 1 shows an example of one of the sequences. The map is built with a resolution of 10 cm. Each integration of sensor data takes on average 40 ms using a single CPU thread. Additional detailed views can be seen in Figure 2.

A. Dataset

SemanticKITTI adds point-wise semantic and instance labels to KITTI Odometry [51], a large scale dataset for autonomous driving. The dataset is sequential, and all scans were recorded using Velodyne HDL-64E LiDAR at 10 hz. It contains 23 201 training and 20 351 testing scans, annotated with 25 semantic classes.

¹<https://github.com/UnknownFreeOccupied/ufomap>

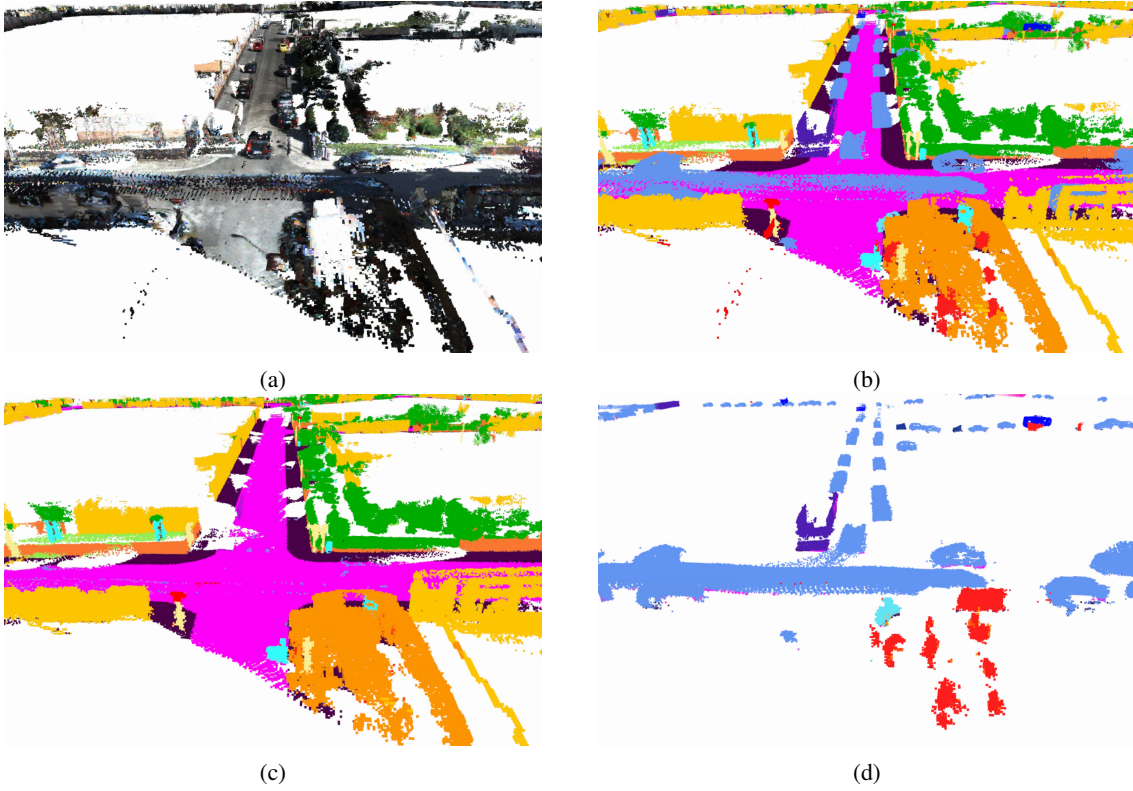


Fig. 5: Rendering occupied voxels from UFOMap at 10 cm resolution on SemanticKITTI [6] dataset, sequence 07. (a) Color and (b) Semantic information respectively for the entire scene. (c) Background and (d) Foreground objects.

TABLE I: LiDAR based semantic segmentation evaluation using a map compared to single scan, in percent.

	mIoU	Car	Bicycle	Motorcycle	Truck	Other-vehicle	Person	Bicyclist	Motorcyclist	Road	Parking	Sidewalk	Other-ground	Building	Fence	Vegetation	Trunk	Terrain	Pole	Traffic sign
SPVNAS [52]	62.9	96.5	32.6	64.1	68.5	58.1	69.9	83.5	0.0	93.2	48.2	80.6	0.0	91.1	64.2	88.1	66.6	74.5	64.1	50.8
UFOMap ^{top-1} _{SPVNAS}	64.1	96.0	39.5	67.7	82.9	66.4	74.0	83.2	0.0	91.8	48.8	78.2	0.0	91.1	62.3	87.3	63.5	72.0	62.6	50.1
SPVCNN [52]	61.4	96.5	17.0	60.2	72.2	56.5	66.0	81.0	0.0	93.3	46.5	80.1	0.0	91.2	63.3	89.0	65.6	76.8	64.1	47.4
UFOMap ^{top-1} _{SPVCNN}	62.7	96.0	18.6	64.8	86.9	66.5	71.3	82.3	0.0	92.2	45.5	78.0	0.0	91.4	62.0	88.5	63.1	75.4	62.7	45.6
UFOMap ^{top-1} _{fusion}	65.1	96.8	28.6	69.4	85.5	70.4	73.7	85.3	0.0	92.9	48.5	80.0	0.0	92.2	67.0	88.6	67.6	75.4	64.5	50.9

B. Map Manipulation and Runtime Comparison

In this section, we show some qualitative results on how UFOMap can be used to manipulate map information. We also compare its runtime performance with OctoMap [35].

C. Semantic Segmentation Using Information Fusion

In this section, we evaluate the hypothesis that a 3D grid is beneficial for information fusion. Concretely, we take off-the-shelf DNN based approaches for LiDAR-based semantic segmentation and fuse their single scan semantic estimates across time using UFOMap. Thereafter, we evaluate if doing so helps improve the overall semantic segmentation. For our baseline, we choose SPVNAS and SPVCNN [52] neural networks, motivated by their top performance on the semantic segmentation benchmark.

Evaluation is carried out on the validation set (sequence 8) of the SemanticKITTI dataset, containing 4071 scans. Following the official SemanticKITTI benchmark, we evaluate on 19 semantic classes and use the mean Jaccard Index shown in Equation 3, also known as the mean intersection over union (IOU) as the metric [53].

$$\frac{1}{C} \sum_{c=1}^C \frac{TP_c}{TP_c + FP_c + FN_c} \quad (3)$$

here TP_c , FP_c and FN_c respectively are the true positive, false positive, and false negative estimates for semantic class c , and C is the total number of classes.

As estimates are accumulated temporally, a single voxel might encounter hits from multiple scans. As output we first

integrate the measurements (semantic estimates) until time step t into UFOMap. Then for each point at time step t , we query the voxel that it belongs to for the label with highest confidence. Depending on the resolution of the map, the sequence, and the network we used, we observed that up to 15 % of voxels can have two or more labels with the same highest confidence. In these cases, we pick the label from the neural network to break the tie. We refer to this output as $\text{UFOMap}^{\text{top-1}}$.

To investigate the information fusion capabilities of the map, we also fuse the semantic estimates from SPVCNN and SPVNAS. That is, each point in the input point cloud now contains two labels, corresponding to the top-1 labels of the two networks. We refer to it as $\text{UFOMap}_{\text{fusion}}^{\text{top-1}}$.

VII. EXPERIMENTAL RESULTS

A. Semantic Segmentation Using Information Fusion

Table I shows the results from Section VI-C. We observe that accumulating information in UFOMap shows a marginal improvement in the mean IOU, when compared to single scan estimates from the networks. Notably, fusing estimates from the two networks further improves the results, without the need for additional expensive labelling and neural network training.

The IOU improves for foreground classes (movable objects), indicating that fusing the estimates is beneficial for classes which are statistically less represented in the point cloud. On the other hand, the IOU becomes worse for the background classes (static objects). The foreground objects are more likely to be surrounded by free space; hence all the points in surrounding area are likely to have the same label. On the other hand, the background classes often share borders. Hence when querying in these regions, voxelization could lead to mismatch in semantics. Decreasing voxel size should reduce this mismatch, but at same time will lead to worsening performance for foreground objects, due to the reduced accumulation effect.

Notably, even though we only integrate the top-1 label from the network in a voxel at each iteration, a distribution is still formed in the map. That is, each voxel can store multiple semantic labels. This suggests that better estimates can be extracted by, for example, incorporating geometric information or clustering and smoothing techniques.

B. Map Manipulation and Runtime Comparison

In the top row of Figure 5 we see the color and semantic information for a section of the map. We can efficiently extract, for example, background/foreground objects (bottom row). Using queries based on semantics, one can easily obtain representations tailored to different use cases. For instance, similar to [13], one can retain the observable elements in the surroundings (e.g. buildings, pole-like objects, traffic lights), to obtain a map usable for localization.

Occlusions play an important role in assessing risk for autonomous vehicles. UFOMap provides mechanisms for finding such regions. Using the time step indicator, as shown in Figure 4, one can look at voxels that have not been updated

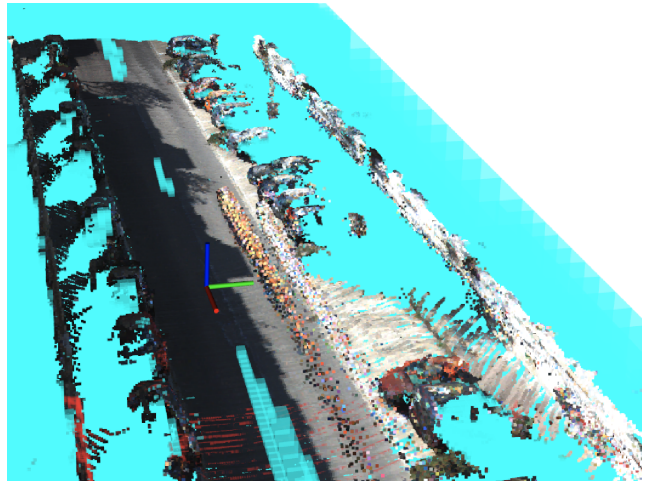


Fig. 6: Showing part of map while building it. The axes represent the ego vehicle, traveling upwards. The parts marked in cyan are either old (based on the time step stored in the voxels) or unknown information. As can be seen, space behind the ego vehicle is classified as unknown again.

since a certain time. Furthermore, we can include the cells that are in the unknown state. Figure 6 shows a snapshot of a scene where all voxels that are occluded are marked in cyan.

Figure II lists the computational performance averaged over a sequence containing 4540 scans. UFOMap far exceeds OctoMap in terms of the memory efficiency, the time taken to integrate measurements into the map, as well as publishing the map to distribute it for use by different components. OctoMap publishes the entire map at every iteration, making it prohibitively slow. For this experiment, the publishing rate for OctoMap was reduced to once every hundred iterations. In comparison, UFOMap publishes only the updated part of the map, making the publishing at each iteration scalable. Notably at any time, the end result remains the same at the receiving end, i.e., the entire map of the environment.

Furthermore, we query for all unknown voxels at 20 cm resolution within a $200 \times 200 \times 10 \text{ m}^3$ axis aligned bounding box around the vehicle. For UFOMap we can directly query for the unknown voxels, or those which haven't been updated within the last 5 seconds, leading to a significant speedup. Exploiting the hierarchical nature of the map can also be beneficial. For example, for 10 cm resolution we query for unknown space one level up the tree, and for 20 cm resolution we do this at leaf level; hence, in both cases we effectively query for information at 20 cm.

TABLE II: Single threaded performance on sequence 00.

Map	Res. (cm)	Mem. (GiB)	Integrate (s)	Publish (s)	Query (s)
UFOMap	10	1.14	0.05(1)	0.04(1)	0.07(4)
OctoMap		9.46	1.62(31)	20.65(1095)	1.75(28)
UFOMap	20	0.43	0.03(1)	0.01(1)	0.06(3)
OctoMap		1.48	0.41(10)	3.49(185)	1.69(25)

VIII. SUMMARY AND CONCLUSIONS

In this paper, we provide a comprehensive review of existing map representations for autonomous driving. Furthermore, we introduced UFOMap as a way to achieve real-time semantic 3D mapping for outdoor environments.

At the moment, UFOMap does not handle dynamic objects well. This can be observed in Figure 6, where two cyclists enter the scene, thus inducing noise. Incorporating the dynamic behavior of the environment into our framework is the next step in the research. Finally, as we described in Section VII-A there are several directions to investigate to improve the semantic segmentation results. Instead of using the best estimate provided by the neural network, one could consider incorporating the distribution over all semantic classes, using an integration model similar to [39]. Fusing estimates from multiple sensor modalities for semantic segmentation networks should also prove beneficial.

REFERENCES

- [1] G. Bresson, Z. Alsayed, L. Yu, and S. Glaser, “Simultaneous localization and mapping: A survey of current trends in autonomous driving,” *IEEE T-IV*, vol. 2, no. 3, 2017.
- [2] E. Yurtsever, J. Lambert, A. Carballo, and K. Takeda, “A survey of autonomous driving: Common practices and emerging technologies,” *IEEE access*, vol. 8, 2020.
- [3] J. Fei, K. Peng, P. Heidenreich, F. Bieder, and C. Stiller, “Pillarsegnet: Pillar-based semantic grid map estimation using sparse lidar data,” in *2021 IEEE Intelligent Vehicles Symposium (IV)*, 2021, pp. 838–844.
- [4] B. R. Kiran, L. Roldão, B. Irastorza, R. Verastegui, S. Süß, S. K. Yogamani, V. Talpaert, A. Lepoutre, and G. Trehard, “Real-time dynamic object detection for autonomous driving using prior 3d-maps,” in *ECCV Workshops*, 2018.
- [5] K. Kim, S. Cho, and W. Chung, “Hd map update for autonomous driving with crowdsourced data,” *IEEE Robotics and Automation Letters*, vol. 6, no. 2, pp. 1895–1901, 2021.
- [6] J. Behley, M. Garbade, A. Milioto, J. Quenzel, S. Behnke, C. Stachniss, and J. Gall, “Semantickitti: A dataset for semantic scene understanding of lidar sequences,” in *Proceedings of the IEEE/CVF International Conference on Computer Vision*, 2019, pp. 9297–9307.
- [7] D. Duberg and P. Jensfelt, “Ufomap: An efficient probabilistic 3d mapping framework that embraces the unknown,” *IEEE Robotics and Automation Letters*, vol. 5, no. 4, 2020.
- [8] M. Yang, S. Wang, J. Bakita, T. Vu, F. D. Smith, J. H. Anderson, and J.-M. Frahm, “Re-thinking cnn frameworks for time-sensitive autonomous-driving applications: Addressing an industrial challenge,” in *RTAS*, IEEE, 2019.
- [9] R. Liu, J. Wang, and B. Zhang, “High definition map for automated driving: Overview and analysis,” *Journal of Navigation*, 2019.
- [10] P. Bender, J. Ziegler, and C. Stiller, “Lanelets: Efficient map representation for autonomous driving,” in *IVSP*, IEEE, 2014.
- [11] D. Paz, H. Zhang, Q. Li, H. Xiang, and H. I. Christensen, “Probabilistic semantic mapping for urban autonomous driving applications,” in *IEEE/RSJ International Conference on Intelligent Robots and Systems*, 2020, pp. 2059–2064.
- [12] M. Dupuis, M. Strobl, and H. Grezlikowski, “Open-drive 2010 and beyond—status and future of the de facto standard for the description of road networks,” in *Proc. of the Driving Simulation Conference Europe*, 2010, pp. 231–242.
- [13] F. Poggenhans, J.-H. Pauls, J. Janosovits, S. Orf, M. Naumann, F. Kuhnt, and M. Mayr, “Lanelet2: A high-definition map framework for the future of automated driving,” in *ITSC*, 2018.
- [14] M. Naumann, H. Königshof, M. Lauer, and C. Stiller, “Safe but not overcautious motion planning under occlusions and limited sensor range,” in *Intelligent Vehicles Symposium (IV)*, IEEE, 2019, pp. 140–145.
- [15] R. Queiroz, T. Berger, and K. Czarnecki, “Geoscenario: An open dsl for autonomous driving scenario representation,” in *Intelligent Vehicles Symposium (IV)*, IEEE, 2019, pp. 287–294.
- [16] M. Althoff, M. Koschi, and S. Manzingier, “Commonroad: Composible benchmarks for motion planning on roads,” in *Intelligent Vehicles Symposium (IV)*, IEEE, 2017, pp. 719–726.
- [17] W. Zhan, L. Sun, D. Wang, H. Shi, A. Clausse, M. Naumann, J. Kummerle, H. Königshof, C. Stiller, A. de La Fortelle, *et al.*, “Interaction dataset: An international, adversarial and cooperative motion dataset in interactive driving scenarios with semantic maps,” *arXiv preprint arXiv:1910.03088*, 2019.
- [18] D. DeTone, T. Malisiewicz, and A. Rabinovich, “Superpoint: Self-supervised interest point detection and description,” in *Proceedings of the IEEE conference on computer vision and pattern recognition workshops*, 2018, pp. 224–236.
- [19] J. Tang, R. Ambrus, V. Guizilini, S. Pillai, H. Kim, P. Jensfelt, and A. Gaidon, “Self-Supervised 3D Key-point Learning for Ego-Motion Estimation,” in *Conference on Robot Learning (CoRL)*, 2020.
- [20] P.-E. Sarlin, A. Unagar, M. Larsson, H. Germain, C. Toft, V. Larsson, M. Pollefeys, V. Lepetit, L. Hammarstrand, F. Kahl, *et al.*, “Back to the feature: Learning robust camera localization from pixels to pose,” in *Proceedings of the IEEE/CVF Conference on Computer Vision and Pattern Recognition*, 2021, pp. 3247–3257.
- [21] N. Jonnavithula, Y. Lyu, and Z. Zhang, “Lidar odometry methodologies for autonomous driving: A survey,” *arXiv preprint arXiv:2109.06120*, 2021.

- [22] J. Zhang and S. Singh, "Loam: Lidar odometry and mapping in real-time," in *Robotics: Science and Systems*, Berkeley, CA, vol. 2, 2014, pp. 1–9.
- [23] —, "Visual-lidar odometry and mapping: Low-drift, robust, and fast," in *IEEE International Conference on Robotics and Automation*, 2015, pp. 2174–2181.
- [24] X. Zheng and J. Zhu, "Efficient lidar odometry for autonomous driving," *IEEE Robotics and Automation Letters*, vol. 6, no. 4, pp. 8458–8465, 2021.
- [25] J. Behley and C. Stachniss, "Efficient surfel-based slam using 3d laser range data in urban environments," in *Robotics: Science and Systems*, vol. 2018, 2018, p. 59.
- [26] H. Moravec and A. Elfes, "High resolution maps from wide angle sonar," in *Proceedings. 1985 IEEE ICRA*, vol. 2, 1985.
- [27] C. Badue, R. Guidolini, R. V. Carneiro, P. Azevedo, V. B. Cardoso, A. Forechi, L. Jesus, R. Berriel, T. M. Paixao, F. Mutz, *et al.*, "Self-driving cars: A survey," *Expert Systems with Applications*, vol. 165, p. 113 816, 2021.
- [28] R. W. Wolcott and R. M. Eustice, "Robust lidar localization using multiresolution gaussian mixture maps for autonomous driving," *The International Journal of Robotics Research*, vol. 36, no. 3, pp. 292–319, 2017.
- [29] C. Montani and R. Scopigno, "Rendering volumetric data using the sticks representation scheme computer graphics," in *ACM SIGGRAPH Computer Graphics*, 1990.
- [30] H. Badino, U. Franke, and D. Pfeiffer, "The stixel world-a compact medium level representation of the 3d-world," in *Joint Pattern Recognition Symposium*, Springer, 2009.
- [31] T. M. Hehn, J. F. P. Kooij, and D. M. Gavrilu, "Instance stixels: Segmenting and grouping stixels into objects," in *IEEE IV*, 2019.
- [32] H. Caesar, V. Bankiti, A. H. Lang, S. Vora, V. E. Liong, Q. Xu, A. Krishnan, Y. Pan, G. Baldan, and O. Beijbom, "Nuscenes: A multimodal dataset for autonomous driving," in *CVPR*, 2020.
- [33] M.-F. Chang, J. W. Lambert, P. Sangkloy, J. Singh, S. Bak, A. Hartnett, D. Wang, P. Carr, S. Lucey, D. Ramanan, and J. Hays, "Argoverse: 3d tracking and forecasting with rich maps," in *Conference on Computer Vision and Pattern Recognition (CVPR)*, 2019.
- [34] H. Oleynikova, Z. Taylor, M. Fehr, J. I. Nieto, and R. Siegwart, "Voxblox: Building 3d signed distance fields for planning," *CoRR*, vol. abs/1611.03631, 2016. arXiv: 1611.03631.
- [35] A. Hornung, K. M. Wurm, M. Bennewitz, C. Stachniss, and W. Burgard, "Octomap: An efficient probabilistic 3d mapping framework based on octrees," *Autonomous robots*, vol. 34, no. 3, pp. 189–206, 2013.
- [36] A. Kirillov, K. He, R. Girshick, C. Rother, and P. Dollár, "Panoptic segmentation," in *Proceedings of the IEEE CVPR*, 2019.
- [37] S. Garg, N. Sünderhauf, F. Dayoub, D. Morrison, A. Cosgun, G. Carneiro, Q. Wu, T.-J. Chin, I. Reid, S. Gould, *et al.*, "Semantics for robotic mapping, perception and interaction: A survey," *Foundations and Trends® in Robotics*, vol. 8, no. 1–2, pp. 1–224, 2020.
- [38] M. Aygun, A. Osep, M. Weber, M. Maximov, C. Stachniss, J. Behley, and L. Leal-Taixé, "4d panoptic lidar segmentation," in *Proceedings of the IEEE CVPR*, 2021.
- [39] A. Rosinol, M. Abate, Y. Chang, and L. Carlone, "Kimera: An open-source library for real-time metric-semantic localization and mapping," in *IEEE Intl. Conf. on Robotics and Automation (ICRA)*, 2020.
- [40] G. Narita, T. Seno, T. Ishikawa, and Y. Kaji, "Panopticfusion: Online volumetric semantic mapping at the level of stuff and things," in *2019 IEEE/RSJ IROS*, 2019.
- [41] M. Grinvald, F. Furrer, T. Novkovic, J. J. Chung, C. Cadena, R. Siegwart, and J. Nieto, "Volumetric Instance-Aware Semantic Mapping and 3D Object Discovery," *IEEE Robotics and Automation Letters*, vol. 4, no. 3, pp. 3037–3044, Jul. 2019.
- [42] F. Bieder, S. Wirges, J. Janosovits, S. Richter, Z. Wang, and C. Stiller, "Exploiting multi-layer grid maps for surround-view semantic segmentation of sparse lidar data," *2020 IEEE Intelligent Vehicles Symposium (IV)*, pp. 1892–1898, 2020.
- [43] J. Fei, K. Peng, P. Heidenreich, F. Bieder, and C. Stiller, "Pillarsegnet: Pillar-based semantic grid map estimation using sparse lidar data," *2021 IEEE Intelligent Vehicles Symposium (IV)*, pp. 838–844, 2021.
- [44] Y. Xiang, W. Choi, Y. Lin, and S. Savarese, "Subcategory-aware convolutional neural networks for object proposals and detection," in *WACV, IEEE*, 2017.
- [45] E. Arnold, O. Y. Al-Jarrah, M. Dianati, S. Fallah, D. Oxtoby, and A. Mouzakitis, "A survey on 3d object detection methods for autonomous driving applications," *IEEE Transactions on Intelligent Transportation Systems*, vol. 20, no. 10, pp. 3782–3795, 2019.
- [46] Y. Xiang, W. Choi, Y. Lin, and S. Savarese, "Data-driven 3d voxel patterns for object category recognition," in *Proceedings of the IEEE CVPR*, 2015.
- [47] C. G. Keller, M. Enzweiler, M. Rohrbach, D. F. Llorca, C. Schnorr, and D. M. Gavrilu, "The benefits of dense stereo for pedestrian detection," *IEEE T-ITS*, vol. 12, no. 4, 2011.
- [48] A. Broggi, E. Cardarelli, S. Cattani, and M. Sabbatelli, "Terrain mapping for off-road autonomous ground vehicles using rational b-spline surfaces and stereo vision," in *IEEE IV*, 2013.
- [49] D. Maturana, P.-W. Chou, M. Uenoyama, and S. Scherer, "Real-time semantic mapping for autonomous off-road navigation," in *Field and Service Robotics*, 2018.

- [50] M. Quigley, K. Conley, B. Gerkey, J. Faust, T. Foote, J. Leibs, R. Wheeler, A. Y. Ng, *et al.*, “Ros: An open-source robot operating system,” in *ICRA workshop on open source software*, Kobe, Japan, vol. 3, 2009, p. 5.
- [51] A. Geiger, P. Lenz, and R. Urtasun, “Are we ready for autonomous driving? the kitti vision benchmark suite,” in *conference on computer vision and pattern recognition*, IEEE, 2012, pp. 3354–3361.
- [52] H. Tang, Z. Liu, S. Zhao, Y. Lin, J. Lin, H. Wang, and S. Han, “Searching efficient 3d architectures with sparse point-voxel convolution,” in *European conference on computer vision*, Springer, 2020, pp. 685–702.
- [53] M. Everingham, S. Eslami, L. Van Gool, C. K. Williams, J. Winn, and A. Zisserman, “The pascal visual object classes challenge: A retrospective,” *International journal of computer vision*, vol. 111, no. 1, pp. 98–136, 2015.